Effects of cohesion on the surface angle and velocity profiles of granular material in a rotating drum

Robert Brewster,[1] Gary S. Grest,[2] and Alex J. Levine[3,4]
[1]*Department of Materials and Interfaces, Weizmann Institute of Science, P.O. Box 26, Rehovot 76100, Israel*
[2]*Sandia National Laboratories, Albuquerque, New Mexico 87185, USA*
[3]*Department of Chemistry and Biochemistry, University of California, Los Angeles, California 90095, USA*
[4]*California Nanosystems Institute, University of California, Los Angeles, California 90095, USA*
(Received 16 September 2008; published 30 January 2009)

Large scale, discrete element simulations are performed to study the dynamics of a rotating drum partially filled with cohesive granular particles. The continuous avalanche regime is explored using a simple model for interparticle cohesion in order to simulate the effects of granular media in the presence of a wetting fluid. The shape of the free surface for cohesionless particles ranges from flat to a concave S shape depending on the rotation rate and frictional properties between the grains and the drum side walls. The presence of interparticle cohesion reduces the concavity of the free surface and pushes the free surface towards a flat or even slightly convex shape. From contour plots of the velocity, we show how the position of the vortex core (the stationary spot in the laboratory frame) depends on the rotation speed and interparticle cohesion strength and how this relationship can be understood from considerations of the incompressibility condition on the mass flow.

DOI: 10.1103/PhysRevE.79.011305 PACS number(s): 45.70.Mg, 83.10.Ff

I. INTRODUCTION

Historically the investigation of the dynamics of granular materials has largely been of interest in agricultural and engineering communities. Over the last 2 decades granular matter has also been recognized by physicists as an easily accessible yet complex system that is inherently far from equilibrium. The bulk of these studies have focused on dry granular particles in which steric repulsion is the dominant interparticle interaction. However, in nature and in many particulate matter processing conditions, small amounts of a wetting fluid can lead to adhesive forces between particles. Thus, in order to make contact with the phenomenology associated with granular dynamics in a geophysical or powder processing context, it is important to consider the effects of cohesion between granular particles. From a more fundamental physical point, interparticle adhesion introduces a new length scale in the system associated with the depth in the pile at which the local gravitational stresses equal the cohesive ones. It remains an open question to assess the role of this length scale on granular flows in a variety of geometries.

In this study, we consider the rotating drum. Here, a cylinder is partially filled with the granular material and oriented such that gravity points perpendicular to the long axis of the drum. The cylinder is then rotated about the long axis to induce flow. This flow geometry is both ubiquitous in granular experiments and an important model system used to investigate the kinetics of mixing [1–3] in polydisperse granular systems. The investigation of such mixing problems has important industrial ramifications and a long history of investigation including the now famous "Brazil nut effect" [4]. In the rotating drum both radial [5,30] and axial [6–8] size segregation are observed in experiment and simulation. We comment briefly on the implications of our work for mixing below.

In the rotating drum the angle of free granular surface increases with respect to gravity leading to avalanching. There are two principal regimes of these dynamics controlled by the angular velocity of the drum. At sufficiently low angular velocities, the avalanching is intermittent, showing stick-slip behavior in which the local angle of the free surface changes in time. There have been a number of studies of dry, cohesionless grains in this regime [9–11]. The stick-slip regime has been recently exploited to study the effects of cohesion on static assemblies [12,13] as a direct test of theoretical predictions pertaining to the interparticle forces resulting from wetting fluids [14,15]. At fast enough rotation rates the avalanching becomes continuous and the shape of the free surface time independent [16]. The flow is confined to a thin layer near the free surface, while the bulk of the material moves in solid rotation with the drum. The depth of the flowing layer is affected in a complex manner by the presence of end walls and their frictional properties [17–19]. The free surface in the continuously avalanching regime is also observed to be curved. At high rotation rates, this curvature is attributed to inertial effects on the flow. Particles emerge from the bulk with appreciable momentum normal to the local free surface. This results in that surface assuming an S shape [16,21–23].

In this study, we focus on the continuous flow regime and, through discrete element simulations, explore the effects of interparticle cohesive forces (such as those due to the presence of a wetting fluid) on the flow properties. We show how this interparticle cohesion mitigates the effect of inertia in that it drives the free surface towards a flat and, for strong enough cohesion, even a slightly convex shape. In addition, we show how the depth of flow at the center of the drum depends on both cohesion and rotation rate. Finally, we find that interparticle cohesion creates plug flow near the free surface at the top of the flowing layer. Previously, we reported [24] the formation of plug flow in the inclined plane geometry. In that study, the size of the plug as a function of cohesive strength was predicted by equating the shear stress in the plug due to the weight of the overlying material to the

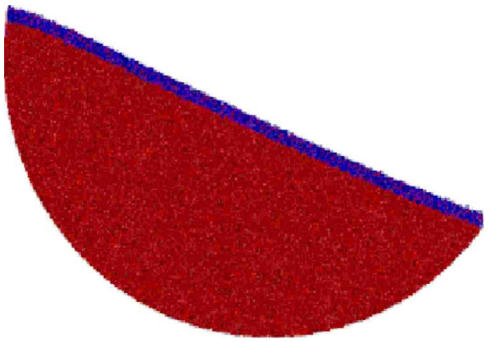

FIG. 1. (Color online) A snapshot of the periodic drum during a simulation with $\omega=1.25\times10^{-3}/\tau$ and $A=0$. For small rotation rates and cohesive strengths, the surface is flat. The particles on the surface are colored blue while those in the interior are colored red. Particles forming the drum wall are not shown for clarity.

predicted yield stress [24]. Here we find that this same relation correctly predicts the plug size both as a function of cohesive strength and free surface angle.

In Sec. II we give the simulation details, including the details of the system's geometry and of the models of the interparticle forces. In Sec. III we present the results of the simulations. Particular emphasis is given to the properties of the free surface and the velocity profiles in the continuous avalanching regime. Finally, we conclude with a summary of the results in Sec. IV.

II. SIMULATION METHOD AND DATA ANALYSIS

We perform large-scale discrete element simulations for N monodispersed spheres of diameter d and mass m in three dimensions. The simulation geometry is a cylinder with frictional walls which is rotated about its horizontal axis at a rate, ω. In all simulations, the cylinder has a radius $R=142d$. We consider two different cases for the width of the drum. Generally, we set the axial width to $20d$ with periodic boundary conditions in this direction (z axis for this study); the flow in this geometry should replicate that at the center of a very long drum, such as those generally used experimentally. The other case corresponds to a relatively thin drum with axial length of $40d$. In this case the drum has end walls with the same coefficient of friction μ as the particles'. Unless otherwise specified, all simulations use the periodic drum. In both cases, the cylinder is filled roughly 40% by volume. For the $40d$ wide cylinder $N=10^6$ while for the periodic drum $N=5\times10^5$. Figure 1 shows a snapshot of the granular particles in the periodic geometry for the simple case of a low rotation rate with no cohesion. The particles on the surface are colored blue while the interior particles are colored red.

Our simulations use a modified version of the model developed by Cundall and Strack [25] and Walton [26] for the interparticle interactions with a modification to the normal force to account for interparticle cohesion as in Refs. [24,27]. The contact forces are modeled through a spring-dashpot interaction for both normal and tangential forces to their line of centers. Two contacting spheres i and j separated by $\mathbf{r}_{ij}=\mathbf{r}_i-\mathbf{r}_j$ with a relative velocity $\mathbf{v}_{ij}=\mathbf{v}_i-\mathbf{v}_j$ have a relative normal compression $\delta_{ij}=d-|\mathbf{r}_{ij}|$. The contact force is modeled with the Hookean force-displacement law for the normal and tangential components and $\mathbf{F}_{ij}=\mathbf{F}_{n_{ij}}+\mathbf{F}_{t_{ij}}$ with

$$\mathbf{F}_{n_{ij}}=\left(k_n\delta_{ij}\mathbf{n}_{ij}-\frac{m}{2}\gamma_n\mathbf{v}_{n_{ij}}\right)+\mathbf{F}_{ij}^{c}(\delta_{ij}), \tag{1}$$

$$\mathbf{F}_{t_{ij}}=\left(-k_t\mathbf{u}_{t_{ij}}-\frac{m}{2}\gamma_t\mathbf{v}_{t_{ij}}\right), \tag{2}$$

where $\mathbf{n}_{ij}=\frac{\mathbf{r}_{ij}}{|\mathbf{r}_{ij}|}$. $k_{n,t}$ and $\gamma_{n,t}$ are the elastic and dissipative constants, $\mathbf{u}_{t_{ij}}$ is the elastic tangential displacement. The magnitude of $u_{t_{ij}}$ is truncated, as necessary, to satisfy the Coulomb yield criterion, $|\mathbf{F}_t|\leq\mu|\mathbf{F}_n|$. The interparticle cohesive force between particles i and j, $\mathbf{F}_{ij}^{c}$, (δ_{ij}), is modeled by introducing a Gaussian potential well centered near the edge of each spherical particle $r_c=d-\ell$. The potential

$$U_{ij}^{c}=-Ae^{-(r_c-|\mathbf{r}_{ij}|)^2/\ell^2} \tag{3}$$

with an effective width $\ell=0.01d$ generates a short-ranged attractive force between particles of the form

$$\mathbf{F}_{ij}^{c}=2A\mathbf{n}_{ij}\frac{(r_c-|\mathbf{r}_{ij}|)}{\ell^2}e^{-(r_c-|\mathbf{r}_{ij}|)^2/\ell^2}. \tag{4}$$

This simple choice for the cohesive interaction captures the essential features of realistic fluid-mediated adhesion while allowing for its strength to be controlled by a single parameter A. The Gaussian form of the cohesive potential is not significant; any short-ranged attractive force acting along the line of centers between two particles in contact should provide an equivalent effect on the flows. Cohesion between particles and the boundaries has the same form as above but with $r_c=d/2-\ell$ and $|r_{ij}|$ is the separation between the wall and the center of mass of the particle in question. It is important to point out that the cohesive force in this model is conservative and, as such, does not capture dissipative effects which may be essential in modeling certain features of lubrication forces.

The total force on the ith particle is the sum of the force from each particle, j, within $1.02d$ of particle i plus the gravitational term,

$$\mathbf{F}_i^{tot}=m_i\mathbf{g}+\sum_j(\mathbf{F}_{n_{ij}}+\mathbf{F}_{t_{ij}}). \tag{5}$$

Results are presented in simulation units. Mass and length have units of m and d, the mass and diameter of one grain, respectively. The fundamental units of force, energy, and time are then mg, mgd, and $\sqrt{d/g}$, where g is the acceleration due to gravity. In this study, we set $k_n=2\times10^5mg/d$, $\gamma_n=50\tau^{-1}$, $k_t=2k_n/7$, $\mu=0.5$, and $\gamma_t=0$. Details on the effects of particle stiffness and dissipative parameters have been presented previously [27–29]. For the Hookean force-displacement law, the energy dissipation per collision can be characterized by the coefficient of restitution, e_n, which depends only on k_n and γ_n. For this set of parameters $e_n=0.88$. Furthermore, the strength of the interparticle cohesion, A, is considered in the range of $0\leq A\leq0.2\ mgd$. The

maximum value produces a force capable of suspending up to 15 particles under gravity. The time step for all simulations is $\delta t = 10^{-4}\tau$.

The direction of the gravity vector is rotated each time step to simulate the rotation of the cylinder; the rotation rates ω range from 5×10^{-4} to 5×10^{-3} in units of $1/\tau$. This makes the largest change in angle per time step $\approx 2\times10^{-4}$ deg/δt. For spheres of diameter $d=1$ mm, these bounds correspond to rotation rates between 3 and 30 rpm. The lower bound of the rotation rate is near the boundary between continuous flow and stick-slip flow, while the upper bound approaches the regime where centrifugal forces become significant in that they are then comparable to the weight of the particles. The drum is allowed to equilibrate over $2\times10^{3}\tau$ and then data is collected over a period of 200τ. For the $40d$ wide cylinder all results are taken from a slice $10d$ thick at the center of the drum.

III. RESULTS

Below we discuss the behavior of the stable surface angle and velocity profiles as we vary the system parameters: the rotational speed of the drum ω and the strength of interparticle cohesion A.

A. Surface angle

The shape of the granular free surface depends on both rotation rate and interparticle cohesion. For cohesionless grains, it is well-known that at low rotation rates, but within the continuously avalanching regime, the surface is essentially flat. As the rotation rate is increased the free surface develops curvature tending towards an inverted S shape. This transition occurs at rotation rates for which the dimensionless Froude number ($F_r = R\omega^2/g$) is much less than unity [see [20,21,23] or solid black line in Fig. 2(a) where $F_r \approx 10^{-3}$]. The shape dependence of the granular free surface upon rotation rate has been attributed to two sources: the frictional forces on the system coming from the end walls of the cylinder [23], and inertial effects [31]. The latter proposed mechanism relies on the fact that grains undergoing essentially rigid body motion near the points where the free granular surface intersects the cylindrical walls of the container have a component of their velocity normal to that free surface. This normal component of the particles' velocity is not instantaneously converted into down-plane motion through collisions with the flowing layer. Thus the upper portion of the free surface must bow outward and the lower portion inward generating the inverted S profile.

Turning to our simulations, we note in Fig. 1 that cohesionless grains at small ω and with no end wall effects do generate an essentially flat free surface. The free surface for a cylinder with frictional end walls and length $40d$ is shown in Fig. 2(a) (black, dashed line); the same system with periodic boundary conditions is also shown for comparison (black solid line) demonstrating that the presence of end walls clearly enhances the curvature of the free surface. The periodic drum (having no end walls) shows a drastic reduction in the curvature of the free surface. However, there remains a residual effect, which we attribute to inertia. We expect that increasing interparticle cohesion should further reduce the curvature of the free surface. One might imagine that the presence of cohesion induces an effective surface tension at the free surface, which serves to inhibit curvature. Indeed, such reduction of curvature is seen in Fig. 2(a); as the interparticle cohesion is increased, the surface flattens. Increasing the rotation rate at fixed A destabilizes the flat surface driving the system towards an inverted S shape. This effect is demonstrated by Fig. 2(b); for any value of the cohesive strength, the S shape can be recovered by increasing the rotation rate. To estimate the magnitude of the surface tension, we note that the cohesive forces are on the scale of the particle weight, $F_c \sim Cmg$ with $0 < C < 15$. The work required to remove one particle from the surface is then $\gamma \sim mg\ell/d^2$ where ℓ is the width of the cohesive well and d^2 is the cross section of one particle. Comparing interparticle cohesive forces to the other forces in the problem (i.e., gravitational, friction, and centrifugal), we see that the cohesive

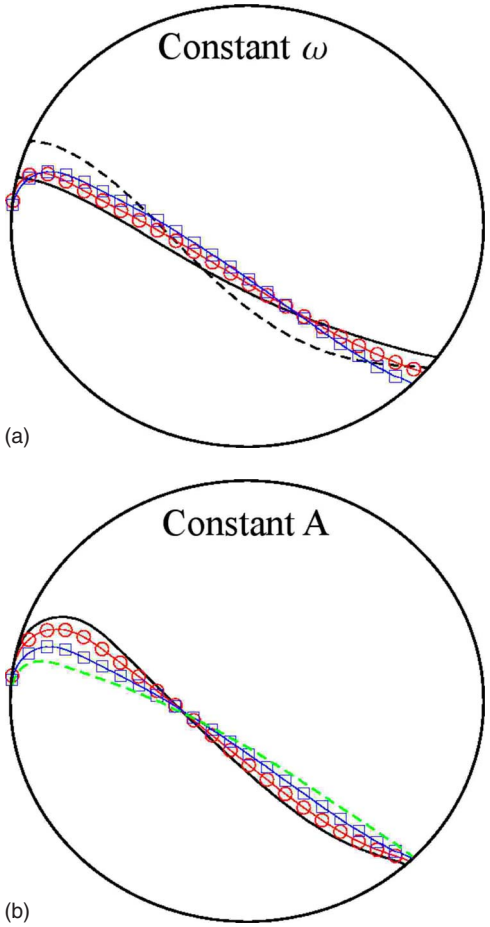

FIG. 2. (Color online) Examples of the shape of the free surface for the periodic drum with (a) fixed rotation rate, $\omega = 2.5\times10^{-3}/\tau$ and $A=0.0$ (black solid line), $A=0.1\ mgd$ (red circles), and $A=0.2\ mgd$ (blue boxes); (b) fixed cohesive strength, $A=0.2\ mgd$, with $\omega = 0.625\times10^{-3}/\tau$ (green dashed line), $\omega = 2.5\times10^{-3}/\tau$ (blue boxes), $\omega = 4\times10^{-3}/\tau$ (red circles), and $\omega = 5\times10^{-3}/\tau$ (black solid line). For comparison, in (a) the black dashed line shows data for the $40d$ wide drum with $\omega = 2.5\times10^{-3}/\tau$ and $A=0.0$.

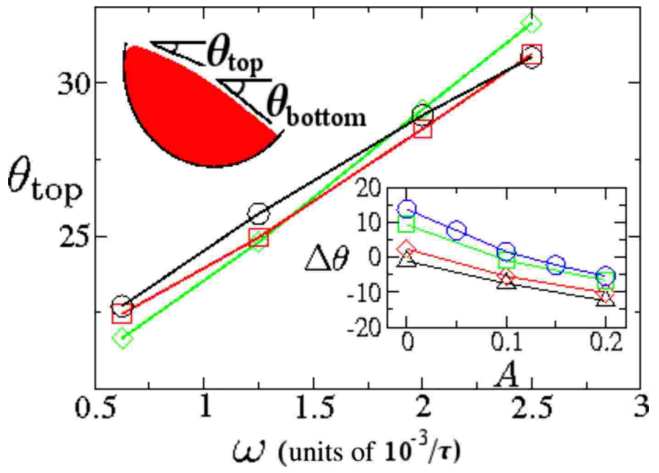

FIG. 3. (Color online) The stable angle in the upper section of the drum, θ_{top}, vs ω with $A=0$ (green diamonds), $A=0.1$ *mgd* (red squares), and $A=0.2$ *mgd* (black circles). Upper inset: schematic picture of how the slope is measured in the top and bottom section of the drum, pictured here for $A=0.2$ and $\omega=0.625\times10^{-3}/\tau$. Lower inset: $\Delta\theta$ vs A for $\omega=0.625\times10^{-3}/\tau$ (black triangles), $\omega=1.25\times10^{-3}/\tau$ (red diamonds), $\omega=2.0\times10^{-3}/\tau$ (green squares), and $\omega=2.5\times10^{-3}/\tau$ (blue circles). Increasing the interparticle cohesion reduces the concave shape of the free surface at larger rotation rates.

forces are of a magnitude to have a significant effect on the shape of the free surface.

We now consider the shape of the free surface in the regime of lower rotation rates (remaining within the continuously avalanching regime): For cohesionless grains, $A=0$, the surface loses curvature with decreasing ω going from a concave interface to a flat one. Cohesive grains, however, develop a *convex* interface at these low rotation rates. This, again, is intuitively reasonable in the framework of an effective granular surface tension due to interparticle cohesion. Recalling that the "three phase" contact line at which the free surface intersects the cylinder is not pinned, one would expect that increasing surface tension would generate a convex interface as the granular material attempts to reduce its free surface area at constant granular volume.

To quantify the convexity of the surface in cohesive sand, we identify regions of approximately constant slope and measure the local angle of inclination with respect to the axis perpendicular to both gravity and the axis of rotation. Generally, such regions are found in both the upper and lower parts of the interface (left and right side in Figs. 1 and 2, respectively). This process is shown schematically in the upper left inset of Fig. 3. For low rotation rates and strong adhesion, these two regions each occupy roughly half of the cylinder [see the blue dotted and red dashed lines in Fig. 2(b) or green dot-dashed and blue dashed lines in Fig. 2(a)]. As the rotation rate increases or adhesion decreases, the upper flat region extends across the majority of the interface, while the lower linear region is correspondingly reduced to a "foot" near the lower intersection of the free surface and the cylinder. See the dash-dot line in Fig. 2(a) and the black solid line in Fig. 2(b) for representative examples.

Figure 3 shows the stable angle in the top section of the drum versus rotation rate. Increasing the rotation rates also increases the stable angle for all cases studied. Initially, the surface angle is smallest for the least adhesive case and increases with A. However, the rate of increase in surface angle decreases as the strength of the cohesion is increased. This effect has also been seen in experiments [32]. For low rotation rates there must be negligible inertial effects, and the surface shape is flat or slightly convex for all values of A. As ω is increased so that the particles' inertia affects the shape of the free surface, the top steady-state angle generically increases—see Fig. 3. The rate of that increase, however, is dependent upon the degree of interparticle cohesion. As A is increased the top steady-state angle increases more slowly with ω: Returning to Fig. 3, we note that the slope of the essentially linear dependence of θ_{top} upon ω *decreases* with increasing cohesion (value of A).

These results can be understood as follows. There is a competition of effects between ω which tends to drive the surface shape towards a concave, inverted S shape as it is increased, and the interparticle cohesion which drives the surface shape towards a convex shape due to an effective granular surface tension. The inset in Fig. 3 shows the difference between the measured stable angle near the top half of the pile and the angle at the bottom half of the pile, $\Delta\theta=\theta_{top}-\theta_{bottom}$, for several values of ω. The crossover from a convex to a concave free surface occurs for larger rotation rates as A is increased. In other words, for higher rotation rates the interparticle cohesion must be stronger to negate the inertial effects caused by particles leaving the free surface when emerging from the bulk.

B. Velocity profiles

In Fig. 4, we show the velocity vector plot for $A=0.1$ *mgd* and two rotation speeds. The closed red circle corresponds to the vortex core, which is the point where the velocity is zero in the laboratory frame. The black cross corresponds to the axis of rotation for the drum. The flowing layer is easily distinguishable from the bulk, solid rotation regime, by which we mean the parts of the pile executing collective rigid body motion.

First we quantify the vortex depth δ defined to be the shortest distance from the vortex core to the surface. We plot data for δ/R as a function of the interparticle cohesion strength A at several rotation rates in Fig. 5. As the strength of the cohesive force increases δ also increases. This trend makes intuitive sense from the consideration of conservation of mass in the flow.

Consider the net flow of mass across a radial line emanating from the cylinder's axis of rotation and passing through the vortex core. The particle current crossing this line must vanish in steady state so

$$\int_0^R v_\theta(r)dr=0, \tag{6}$$

but this integral can be broken up into two pieces corresponding to the integral from the rotation axis to the vortex core at $r=R_v$, and the integral from that point to the outer edge of the cylinder at $r=R$. Rewriting Eq. (6) in this way,

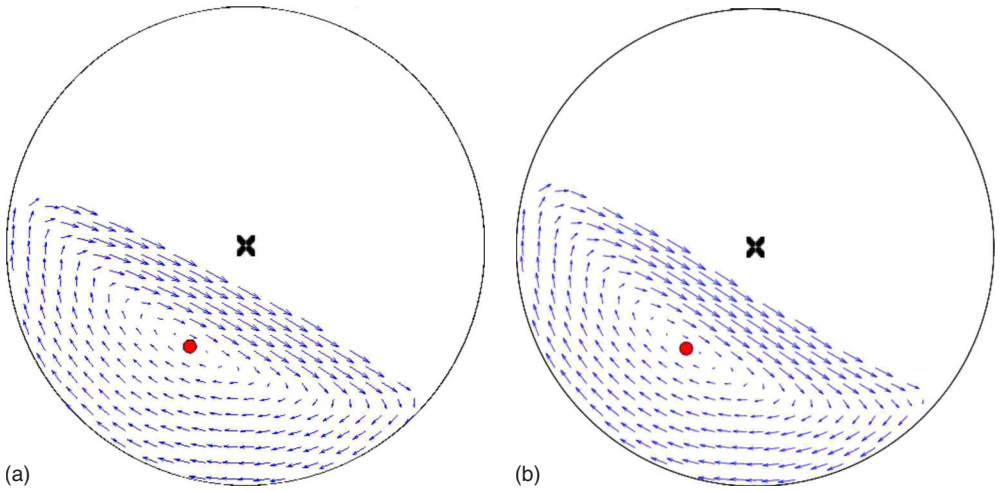

FIG. 4. (Color online) Velocity profiles for $A=0.1\ mgd$ for (a) $\omega=1.25\times10^{-3}/\tau$ and (b) $\omega=2.5\times10^{-3}/\tau$. The axis of the drum is marked with a black "×" and the vortex core is marked by a closed red circle. The vortex core is the point where the magnitude of the velocity is smallest in the laboratory frame.

$$\int_0^{R_v} v_\theta(r)dr = -\int_{R_v}^{R} v_\theta(r)dr, \tag{7}$$

we note that the integral on the left-hand side of Eq. (7) is over a strictly positive quantity and is the mass transported down the incline; the integral over the right side, which is strictly negative, represents the mass transported back up by the rotation of the cylinder.

The presence of cohesion slows the resulting surface flow decreasing $v_\theta(r)$ in the integrand on the left side of Eq. (7). The cohesive forces do not effect the velocity of the material in solid rotation, which makes up the majority of the flow below the vortex core. The tangential velocity field integrated over on the right side of Eq. (7) is not significantly changed by cohesion. Therefore, to maintain the equality of these two integrals in the presence of increasing cohesion, it follows that R_v must increase; the vortex core moves deeper within the pile. Examining our data and reading from low to high rotation rates and at constant A, we see that the rate at which δ increases slows considerably as A increases. This result has also been observed experimentally by Xu *et al.* [32].

In Fig. 6 we show tangential velocity v_θ as a function of r along a radial line connecting the center of rotation of the drum ($r=0$) to the vortex core with $v_\theta=0$. These data are shown for various values of ω at constant A and for various values of A at constant ω. For $A=0$, two regions of flow can be seen. Near the outer edge of the cylinder (large r) the grains move collectively as a solid in rigid body rotation so that $v_\theta=\omega\times r$ (see inset). At smaller values of r, the material undergoes a constant shear deformation. This flowing region extends through the vortex core and up to the free surface. As A or ω is increased, the size of the region above that in solid rotation increases. Additionally, for nonzero values of A another plugged region forms on the free surface, the size of

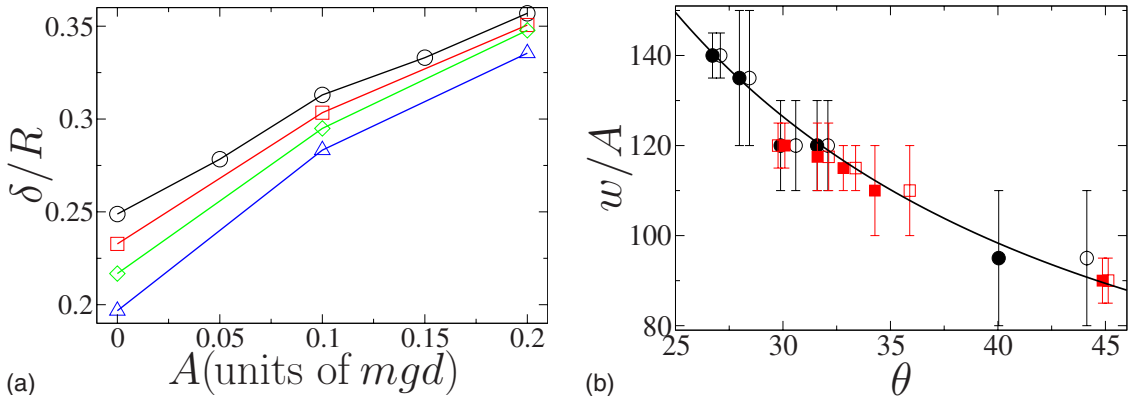

FIG. 5. (Color online) (a) Depth of the flowing layer normalized by the radius of the drum, δ/R versus the strength of interparticle cohesion, A, for $\omega=0.625\times10^{-3}/\tau$ (blue triangles), $\omega=1.25\times10^{-3}/\tau$ (green diamonds), $\omega=2\times10^{-3}/\tau$ (red squares), and $\omega=2.5\times10^{-3}/\tau$ (black circles). (b) Size of the surface plug normalized by the strength of the cohesive interactions versus surface angle. The (black) circles represent data for $A=0.1$ and the (red) squares for $A=0.2$. The open symbols use the local angle at the middle of the drum (where the plug size is measured) and the closed symbols represent the surface angle as measured over the entire free surface. The (black) line is the theoretical prediction for the plug size [Eq. (8)].

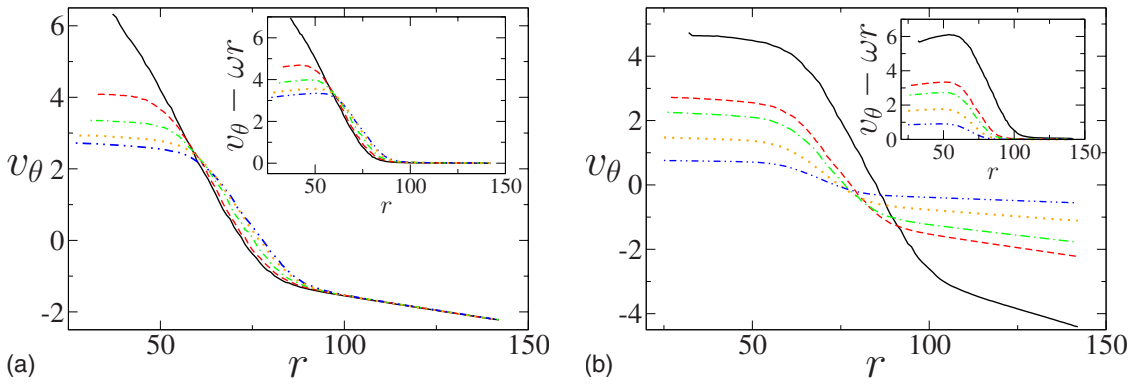

FIG. 6. (Color online) Angular velocity profile versus radius from the drum's center of rotation along the radial line which intersects the vortex core (v_θ=0) for (a) $\omega=2.5\times10^{-3}/\tau$ with $A=0$ (black solid line), $A=0.05$ *mgd* (red dashed line), $A=0.1$ *mgd* (green dot-dashed line), $A=0.15$ *mgd* (gold dotted line), $A=0.2$ *mgd* (blue double dot-dashed line) and (b) $A=0.2$ *mgd* with $\omega=0.625\times10^{-3}/\tau$ (blue double dot-dashed line), $\omega=1.25\times10^{-3}/\tau$ (gold dotted line), $\omega=2\times10^{-3}/\tau$ (green dot-dashed line), $\omega=2.5\times10^{-3}/\tau$ (red dashed line), and $\omega=5\times10^{-3}/\tau$ (black solid line). With increasing A, the flowing region gets larger as slip begins closer to the cylinder wall. Inset to (a) and (b) shows the result of subtracting the rotational portion of v_θ, the regime in solid rotation at the outer wall of the cylinder is easily identified in this frame.

which depends on the cohesion strength and the rotation rate. For the slowest rotation rate in Fig. 6(b) (yellow line) almost the entire system takes part in the rigid body rotation below the vortex core (i.e., at larger r) or is part of the plug flow associated with the free surface.

Surface plug flow was also seen in simulations on inclined plane flow [24] using the same model for the cohesive force. The plug forms near the free surface because the shear stress due to the weight of the overlying material is not enough to overcome the finite yield stress resulting from cohesive force. The thickness of the plug can be calculated by equating the gravitational shear stress (increasing linearly with depth into the pile) to the critical yield stress computed from the maximum cohesive force and the mean number of interparticle contacts. From this analysis we derive in Ref. [24] an expression for the depth of the surface plug w as a function of the cohesion strength, A, and the surface angle, θ,

$$w = \frac{A}{\ell \sin\theta}\frac{e-1}{e}, \tag{8}$$

where e is the base of the natural logarithm and ℓ is the width of the Gaussian attractive potential—see Eqs. (3) and (4). The dependence on A was shown to hold well for chute flow. Figure 5(b) shows data for the plug size w directly above the vortex core versus surface angle for two different cohesion strengths for the rotating drum. The plug size is determined from examination of the shear profile. As already discussed, the surface angle is not constant over the entire length of the free surface. The open symbols in Fig. 5(b) use the surface angle above the vortex core, which is most consistent with our measurement of w. The closed symbols are a measurement of the angle using the entire range of the free surface. In a sense, this gives an upper bound on the uncertainty in measuring θ which is relatively small for most of the data. The angular dependence of the plug size predicted in Eq. (8) (black line in Fig. 5), which is controlled here by the rotation rate, is quite robust.

IV. SUMMARY

We have presented results from large-scale discrete element simulations for damp or otherwise cohesive granular material in a rotating drum. Within the continuously avalanching regime, we have focused on the effects of cohesion strength and rotation rate on the shape of the free surface, the depth of the flowing layer, and, more generally, on the velocity field within the granular media. This makes use of one of the great advantages of numerical simulation in the study of granular flows—the ability to characterize the velocity field in the interior of the system.

We find that the shape of the free surface can be varied by a combination of the rotation rate of the drum and cohesiveness of the particles. At low enough rotation rates and high enough interparticle cohesion, the free surface is convex. Decreasing the cohesion or increasing the rotation rate causes the free surface to flatten. For low enough cohesion and high enough rotation rates the surface assumes an inverted S shape, or in other words, becomes concave. We attribute this behavior to the competition between interparticle cohesion (generating an effective surface tension for the granular material) causing convexity and a combination of granular inertia and the frictional effects of the end walls in creating a concave free surface. Based on a comparison of the shape of the free surface between an infinite length cylinder (periodic boundary conditions) and a finite one (of length 40d) we find that the end wall effect is the dominant driving force towards surface concavity, at least for these relatively short cylinder lengths. One avenue left unexplored is the relative strength of cohesive interactions of particles with the drum walls which may have a strong influence on the shape of the free surface.

We characterize the shape of the surface by the steady-state angle over the upper region and the lower region, where the individual sections can be well-described by a constant slope. We find that while the angle in the upper region starts higher for the cohesive cases, the angle of the upper section, θ_{top}, increases slower than in the dry case. This is in agree-

ment with experimental findings [32] and is due to the suppression of inertial effects by cohesion. In addition, the transition from a flat or slightly convex surface to an inverted S shape (where inertial effects dominate) is observed to occur at larger rotation rates for larger values of A. Taken together, the analysis of the change in the shape of the granular free surface with cohesion and rotation rate suggests that the introduction of an effective surface tension for cohesive granular materials may be a useful approach to the continuum level modeling of these materials.

We also examined the velocity field throughout the rotating drum. When no cohesive interactions are present, the flow is as expected with the majority of the particles in uniform rotational motion and a thin flowing layer near the free surface. When cohesion is present, a plug forms on the free surface above the flowing layer. The size of this plug has been previously predicted for inclined plane flow using a simple stress balance argument. We find that this calculation also accurately predicts the size of the plug in the rotating drum geometry as a function of both cohesive strength and surface angle. In addition, we also extract the distance from the free surface to the vortex core δ from these velocity maps. We find that this length generically increases with rotation rate. The rate of increase with rotation rate decreases as A increases, consistent with experiments.

These velocity maps have implications for the efficacy of using a rotating drum to mix heterogeneous granular materials. While the general problem of granular mixing is highly nontrivial, we may draw a few general implications from an examination of the velocity maps within the rotating drum. Within the regions of the system where the grains are collectively undergoing rigid body motion, i.e., either below the vortex core or in the plug, we expect mixing to be strongly suppressed. On the other hand, near the vortex core where there is a large rate of strain, we expect mixing to occur. Thus we expect the efficacy of granular mixing in a rotating drum to be proportional to the volume of the material in which there is a nonvanishing rate of strain. In general for cohesive granular materials, this includes the region of the vortex core and the regions where the free surface meets the cylinder walls. As the cohesive energy is increased the volume where shear occurs surrounding the vortex core decreases so that we expect a small amount of interparticle cohesion to adversely affect mixing.

[1] G. Metcalfe, T. Shinbrot, J. J. McCarthy, and J. M. Ottino, Nature (London) **374**, 39 (1995).
[2] B. A. Peratt and J. A. Yorke, Europhys. Lett. **35**, 31 (1996).
[3] J. M. Ottino and D. V. Khakhar, Annu. Rev. Fluid Mech. **32**, 55 (2000).
[4] A. Rosato, K. J. Strandburg, F. Prinz, and R. H. Swendsen, Phys. Rev. Lett. **58**, 1038 (1987).
[5] F. Cantelaube and D. Bideau, Europhys. Lett. **30**, 133 (1995).
[6] M. B. Donald and B. Roseman, Br. Chem. Eng. **7**, 749 (1962).
[7] S. Das Gupta, D. V. Khakhar, and S. K. Bathia, Chem. Eng. Sci. **46**, 1513 (1991).
[8] K. M. Hill and J. Kakalios, Phys. Rev. E **52**, 4393 (1995).
[9] H. M. Jaeger, C. H. Liu, and S. R. Nagel, Phys. Rev. Lett. **62**, 40 (1989).
[10] Pierre Evesque, Phys. Rev. A **43**, 2720 (1991).
[11] N. Nakagawa and M. Miyata, in *Powders and Grains 2001* (Swets & Zeitlinger, Lisses, 2001), pp. 467 and 470.
[12] P. Tegzes, T. Vicsek, and P. Schiffer, Phys. Rev. Lett. **89**, 094301 (2002).
[13] S. Nowak, A. Samadani, and A. Kudrolli, Nat. Phys. **1**, 50 (2005).
[14] T. C. Halsey and A. J. Levine, Phys. Rev. Lett. **80**, 3141 (1998).
[15] T. G. Mason, A. J. Levine, D. Ertas, and T. C. Halsey, Phys. Rev. E **60**, R5044 (1999).
[16] J. Rajchenbach, Phys. Rev. Lett. **65**, 2221 (1990).
[17] J. E. Maneval, K. M. Hill, B. E. Smith, A. Caprihan, and E. Fukushima, Granular Matter **7**, 199 (2005).
[18] N. A. Pohlman, J. M. Ottino, and R. M. Lueptow, Phys. Rev. E **74**, 031305 (2006).
[19] P. Chen, J. M. Ottino, and R. M. Lueptow, Phys. Rev. E **78**, 021303 (2008).
[20] C. M. Dury, G. H. Ristow, J. L. Moss, and M. Nakagawa, Phys. Rev. E **57**, 4491 (1998).
[21] M. Nakagawa, S. Altobelli, A. Caprihan, E. Fukushima, and E. Jeong, Exp. Fluids **16**, 54 (1999).
[22] A. V. Orpe and D. V. Khakhar, Phys. Rev. E **64**, 031302 (2001).
[23] N. Taberlet, P. Richard, and E. J. Hinch, Phys. Rev. E **73**, 050301(R) (2006).
[24] R. Brewster, G. S. Grest, J. W. Landry, and A. J. Levine, Phys. Rev. E **72**, 061301 (2005).
[25] P. A. Cundall and O. D. L. Strack, Geotechnique **29**, 47 (1979).
[26] O. R. Walton, Mech. Mater. **16**, 239 (1993).
[27] R. Brewster, L. E. Silbert, G. S. Grest, and A. J. Levine, Phys. Rev. E **77**, 061302 (2008).
[28] L. E. Silbert, D. Ertas, G. S. Grest, T. C. Halsey, D. Levine, and S. J. Plimpton, Phys. Rev. E **64**, 051302 (2001).
[29] L. E. Silbert, G. S. Grest, R. Brewster, and A. J. Levine, Phys. Rev. Lett. **99**, 068002 (2007).
[30] C. M. Dury and G. H. Ristow, J. Phys. I **7**, 737 (1997).
[31] M. Nakagawa, S. A. Altobelli, A. Caprihan, and E. Fukushima, *Powders and Grains '97*, edited by R. P. Behringer and J. T. Jenkins (Balkema, Rotterdam, 1997), p. 447-450.
[32] Q. Xu, A. V. Orpe, and A. Kudrolli, Phys. Rev. E **76**, 031302 (2007).